J Adv Ceram

Research Article

A new type of dense silicon nitride-based metamaterial

Lujie Wang[1], Xuejian Liu[2,✉], Qian Qi[3], Dewei Ni[2], Hui Zhang[2], Jie Yin[2], Zhuhui Qiao[1,4,5,✉], Zhengren Huang[2]

Cite this article: Wang L, X. J. Liu, Qi Q, et al. *J Adv Ceram* 2025, **14**(3): 9221037. https://doi.org/10.26599/JAC.2025.9221037

ABSTRACT: Electromagnetic metamaterials have attracted widespread attention because of their unique properties, and the introduction of conductive metals or carbon into an insulating matrix is the main method for preparing metamaterials. Silicon nitride ceramics have become an ideal matrix for electromagnetic metamaterials because of their high degree of insulation, high thermal conductivity, high-temperature resistance, corrosion resistance, and excellent mechanical properties. However, owing to poor sintering activity, chemical incompatibility, thermal expansion mismatch, or second-phase melt agglomeration, it is difficult to prepare dense silicon nitride-based metamaterials without a mechanical pressure-assisted sintering process, which greatly limits their high-performance preparation and industrial application. To address this issue, this work proposes the use of the high melting point metal tungsten as the conductive second phase. Through the control of chemical reactions, analysis, and regulation of the densification process, the materials were fully densified by gas pressure sintering. After the introduction of tungsten, not only did the electrical and thermal conductivity properties of the silicon nitride ceramics improve, but a negative permittivity behavior was also observed when the tungsten content reached 20 vol%. A new type of dense silicon nitride-based metamaterials with great industrial potential was proposed and prepared, which can guide the preparation and industrial application of high-performance metamaterials.

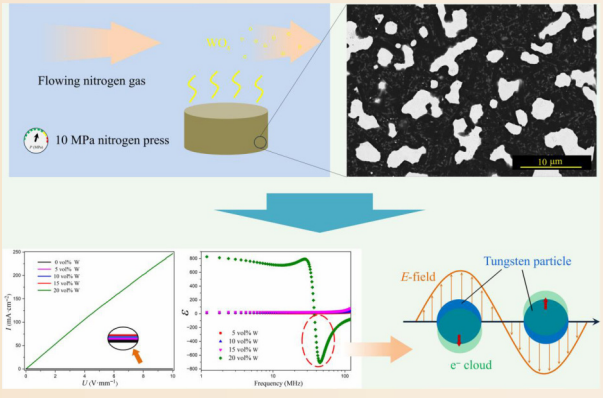

KEYWORDS: electromagnetic metamaterials; silicon nitride; tungsten; negative permittivity.

1 Introduction

Silicon nitride ceramics are known as excellent structural ceramics with comprehensive performance due to their high strength, high toughness, high-temperature resistance, wear resistance, and other characteristics [1]. They are widely used in the preparation of key components such as bearing bushes, bearing balls, and turbine blades [2–5]. Owing to the complexity of service conditions, silicon nitride ceramics are not limited to purely structural materials, and more functionalities are reflected [6]. For example, they are used as substrate materials for IGBT packages because of their high thermal conductivity and high insulating properties [7]. High wave permeability also makes silicon nitride ceramics important materials for missile radomes [8–12]. In recent years, electromagnetic metamaterials with negative permittivity or permeability have shown great potential in the aerospace, medical, communication, and military fields, especially in subwavelength imaging, cloaking, wave filtering, super lens, and band gap design [13–19], and their discovery has been among the top ten advances in materials science in the past 50 years [20]. One of the design concepts of these materials is to introduce randomly distributed conductive phases into the insulating matrix [21], and silicon nitrides have become popular materials for this matrix because of their excellent insulating and mechanical properties [22,23].

To achieve the negative permittivity behavior of silicon nitride ceramics, two main types of additives, including carbon materials such as graphite [22,24,25], carbon fibers [26], and metals such as silver [23] and cobalt [27], have been introduced. The introduction of a large amount of carbon materials results in poor sintering activity of silicon nitride ceramics, while those metals may melt and agglomerate during the sintering of silicon nitride ceramics at high temperatures above 1750 °C. In addition, the large difference in the thermal expansion coefficient and possible chemical reactions between those metals and silicon nitride make

[1] State Key Laboratory of Solid Lubrication, Lanzhou Institute of Chemical Physics, Chinese Academy of Sciences, Lanzhou 730000, China. [2] State Key Laboratory of High Performance Ceramics and Superfine Microstructures, Shanghai Institute of Ceramics, Chinese Academy of Sciences, Shanghai 200050, China. [3] School of Materials Science and Engineering, Shandong University of Science and Technology, Qingdao 266590, China. [4] Shandong Laboratory of Advanced Materials and Green Manufacturing at Yantai, Yantai 264006, China. [5] Yantai Zhongke Research Institute of Advanced Materials and Green Chemical Engineering, Yantai 264006, China.

✉ Corresponding authors. E-mail: X. Liu, xjliu@mail.sic.ac.cn; Z. Qiao, zhqiao@licp.cas.cn

Received: October 23, 2024; Revised: December 23, 2024; Accepted: January 17, 2025

© The Author(s) 2025. This is an open access article under the terms of the Creative Commons Attribution 4.0 International License (CC BY 4.0, http://creativecommons.org/licenses/by/4.0/).

the direct introduction of those metals difficult. To the best of the author's knowledge, there are no reports of the successful introduction of carbon or metal directly into silicon nitride ceramics via pressureless or gas press sintering processes to achieve complete densification of the materials. The current preparation methods for silicon nitride-based metamaterials are limited to pressure-assisted sintering [26] or impregnation of porous ceramics [22–24,27]. Pressure-assisted sintering, such as spark plasma sintering (SPS), can only prepare samples with simple shapes, and the production efficiency is low, which is not suitable for industrialization. In addition, the silicon nitride grains cannot grow sufficiently under these processes, resulting in reduced toughness. In the impregnation process, a silicon nitride ceramic matrix with high porosity is required for the solution to penetrate, which severely deteriorates the mechanical properties, oxidation resistance, and wear resistance of the materials and eliminates the advantages of silicon nitride ceramics. Inorganic conductive particle phases have also been used to prepare metamaterials, but their effectiveness is poor. For example, Xu *et al.* [28] introduced titanium nitride as a conductive phase into polyethylene terephthalate, and only a weakly negative permittivity was observed after the content of titanium nitride reached 69 vol%. Therefore, there is an urgent need to find new additives to prepare silicon nitride-based metamaterials.

In our past study, tungsten particles were found to be metals with a thermal expansion coefficient (4.6×10^{-6} K^{-1}) matching that of silicon nitride ceramics (3.2×10^{-6} K^{-1}) [29]. Although tungsten and silicon nitride react strongly at high temperatures [30], our work revealed that high nitrogen pressure can effectively inhibit these reactions [31], which creates conditions for the direct introduction of tungsten into silicon nitride ceramics. The latest research shows that tungsten particles, as the second phase, can not only effectively improve the fracture toughness of silicon nitride ceramics [32] but also improve the wear resistance of silicon nitride ceramics under different friction pairs [33–35]. More importantly, the high melting point (3370 °C) of tungsten eliminates the problem of melt agglomeration during the sintering process of silicon nitride ceramics, and it does not greatly deteriorate the sintering activity of silicon nitride ceramics such as carbon. After its introduction, the materials can be densified under normal gas pressure sintering processes. To the best of the author's knowledge, there are no reports on the preparation of dense silicon nitride-based metamaterials without mechanical pressure-assisted sintering, which greatly limits the industrial preparation of high-performance metamaterials and their potential applications in harsh working conditions such as oxidizing and corrosive environments.

In this work, tungsten was selected as the conductive phase for the first time to prepare silicon nitride-based metamaterials and silicon nitride ceramics with different tungsten contents were fully densified by gas pressure sintering. The state and distribution of tungsten particles in silicon nitride ceramics were observed and tested. The effects of tungsten particles on the densification process and the thermal and electrical properties of silicon nitride ceramics were analyzed and discussed. Negative permittivity behavior was observed when the tungsten content reached 20 vol%. W/silicon nitride ceramics were proposed as metamaterials for the first time, and negative permittivity behavior was observed for the first time. More importantly, this material has obvious advantages over reported silicon nitride-based metamaterials.

2 Experimental

α-Si_3N_4 powder (metal impurities < 0.01 wt%, 0.5 μm, nitrogen and oxygen contents of 39.1 and 1.2 wt%, respectively) was mixed with 2 vol% alumina (Al_2O_3) powder (1 μm, 99.9 wt%) and 4 vol% yttria (Y_2O_3) powder (1 μm, 99.99 wt%). 5, 10, 15, and 20 vol% W powder (1 μm, 99.95 wt%) was introduced. The mixture was planetary ball milled at 300 RPM for 8 h using absolute ethyl alcohol as a medium. The slurry was dried and sieved into powder and then cold-isostatically pressed at 200 MPa for 10 min to form green samples. The temperature was increased to 1750 °C at a rate of 5 °C·min^{-1} and maintained at that temperature for 2 h to complete the sintering process in an FPW 90 SD gas pressure sintering furnace produced by Fct Systeme Gmbh of Germany. A nitrogen pressure of 10 MPa was maintained throughout the process to suppress the reactions between tungsten and silicon nitride as well as the decomposition of silicon nitride at high temperature. During the sintering process, the green samples were placed in a boron nitride (BN) crucible in a single layer and separated by a certain distance, and a flow of nitrogen through the crucible was used to blow off the volatiles from the sample. A schematic diagram of the sintering process is shown in Fig. 1. The samples without W powder were also prepared for comparison.

This work focused on the permittivity, thermal conductivity, and thermal expansion coefficient of the prepared W/silicon nitride composites. Permittivity is an important criterion for evaluating whether a metamaterial is a metamaterial, and it is also a key performance criterion in application. This also causes Joule heat to be generated during the application process, so heat dissipation and thermal expansion are also issues that must be considered. The phase composition of the sintered samples was analyzed via an X-ray diffraction (XRD) using a Guinier-Hagg camera (Expectron XDC-1000, Jungner Instrument, Sweden) with Cu Kα radiation. The theoretical density was calculated according to the content and theoretical density of each component, and the theoretical densities of Si_3N_4, W, Al_2O_3, and Y_2O_3 were 3.187, 19.300, 3.980, and 5.020 g/cm^3, respectively. The bulk density was measured via the Archimedes method (ASTM C-20). The relative density was determined based on the ratio of the bulk density to the theoretical density. The morphology and elemental distribution of the polished surface of the sample were analyzed via a scanning electron microscope (SEM; Magellan 400, FEI, USA) equipped with an energy dispersive spectrometer (EDS; INCA SERIES, Oxford Instrument, UK). The interface between the tungsten particles and silicon nitride particles was further analyzed via EDS and selected area electron diffraction (SAED) via transmission electron microscope (TEM; Talos F200X G2, Thermo Fisher Scientific, USA). The ultrathin samples were prepared with a focused ion beam (FIB; VERSA 3D, FEI, USA). The coefficient of thermal expansion (CTE) from room temperature to 1200 °C was measured by a dilatometer (DIL 402C, Netzsch Instruments Co. Ltd., Germany), and the tested samples were rectangular bars with dimensions of 24.5 mm ×

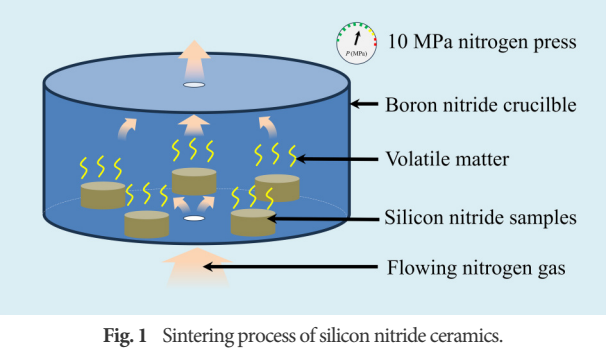

Fig. 1 Sintering process of silicon nitride ceramics.

3 mm × 4 mm. The specific heat and thermal diffusivity from room temperature to 1000 °C was measured by a laser flash diffusivity apparatus (LFA467HT, Netzsch Instruments Co., Ltd., Germany), and pyroceram 9606 was used as a reference material. Eq. (1) was used to calculate the thermal conductivity (κ, $W \cdot m^{-1} \cdot K^{-1}$):

$$\kappa = \rho C \alpha \quad (1)$$

where ρ, C, and α are the bulk density ($g \cdot cm^{-3}$), the specific heat ($J \cdot g^{-1} \cdot K^{-1}$), and the thermal diffusivity ($mm^2 \cdot s^{-1}$), respectively. The electrical conductivity was measured with a DC high-resistance meter (Keithley 6517A, Keithley, USA). The permittivity and impedance of the samples were measured by an impedance analyzer (Agilent 4291B, Agilent Technologies, USA). The samples used for testing the thermal conductivity and electrical properties were cylinders with a diameter of 10 mm and a height of 2 mm. Conductive silver paint was applied evenly on the top and bottom surfaces of the cylindrical sample before the electrical test. All the samples were processed into the required shape and polished in a single-disk automatic polishing machine (AutoPOL GP-1C, Mega Instruments, China) before testing.

3 Results and discussion

3.1 Phase composition and microstructure

The XRD patterns and densities of the samples are shown in Fig. 2. As shown in Fig. 2(a), there are only diffraction peaks of β-Si_3N_4 in monolithic silicon nitride ceramics, whereas the diffraction peaks of tungsten appear with the introduction of tungsten particles. All the α-Si_3N_4 was converted to β-Si_3N_4. Tungsten exists only in the form of a metal, and no other compounds, such as W_5Si_3 or WSi_2, were detected, indicating that tungsten has not reacted with silicon nitride during the sintering process, which was attributed mainly to the high nitrogen gas pressure effectively inhibiting the reactions between tungsten and silicon nitride, as discussed in our past work [31]. For comparison, standard PDFs of α-Si_3N_4 and β-Si_3N_4 have also been added to Fig. 2(a).

Since the density of tungsten is much greater than that of β-Si_3N_4, the bulk density of the samples increases with increasing tungsten content, as shown in Fig. 2(b). To visualize the degree of densification of the sample, the relative density of the sample was also calculated and is shown in the figure. The relative density of all the samples clearly exceeds 98.5%, indicating that all the samples have been fully densified. Nevertheless, this is different from our previous work, where the densification degree of silicon nitride ceramics deteriorated sharply when the tungsten content exceeded 10 vol% [32]. This results from the adjustment of the process. Tungsten particles were slightly oxidized during the introduction process, such as ball milling and sieving, forming a small amount of tungsten oxide on the surface of the W particles. These tungsten oxides were doped into the liquid phase formed by sintering aids during the sintering process. Owing to the high electronegativity of tungsten ions, their doping increased the liquid viscosity and inhibited the particle rearrangement process of liquid-phase sintering. The phenomenon that the introduction of highly electronegative tungsten ions leads to an increase in the viscosity of glass has been confirmed and reported [36,37]. This is the reason for the poor densification degree of the samples with high tungsten contents in our past work. In the present work, as shown in Fig. 1, the green samples were placed in a BN crucible in a single layer and separated by a certain distance, and nitrogen flowing through the crucible was used during the sintering process. Since tungsten oxide easily volatilizes above 900 °C [38], some tungsten oxide is removed by flowing nitrogen before the liquid phase is formed (~1450 °C). Therefore, the samples with high tungsten contents were fully densified. More details have been discussed in our past work [29].

SEM images of polished silicon nitride ceramics with different tungsten contents are shown in Fig. 3. There is no obvious porosity on the polished surface of the sample, regardless of whether the tungsten content is high or low. This indicates that all the samples were fully densified, which is consistent with the density results in Fig. 2(b). In the backscattered electron mode, the brightness of the particle is proportional to the atomic number. According to this phenomenon, combined with the XRD results in Fig. 2(a), the bright particles in Fig. 3 are tungsten particles. As shown in Figs. 3(b)–3(e), the tungsten particles gradually increase with increasing tungsten content, and many tungsten particles are bonded to each other when the tungsten particle content reaches 20 vol%, as shown in Fig. 3(e). Interconnected tungsten particles may have a significant effect on the electrical properties of silicon nitride ceramics. Figure 3(f) is a partially enlarged view of Fig. 3(e), showing a clearer distribution of silicon nitride grains, tungsten grains, and grain boundary phases. SEM-EDS mapping of the polished sample with the introduction of 20 vol% tungsten, as shown in Fig. 4, further confirms the element distribution. In addition, rod-shaped β-Si_3N_4 grains with lengths of nearly 10 μm can be observed on the polished surfaces of all the samples. This shows that under the gas pressure sintering process, the β-Si_3N_4 grains grew to a certain extent even in the presence of many tungsten particles.

To further observe the interface between the silicon nitride particles and tungsten particles, TEM analysis was performed, and the results are shown in Fig. 5. No interface transition layer was

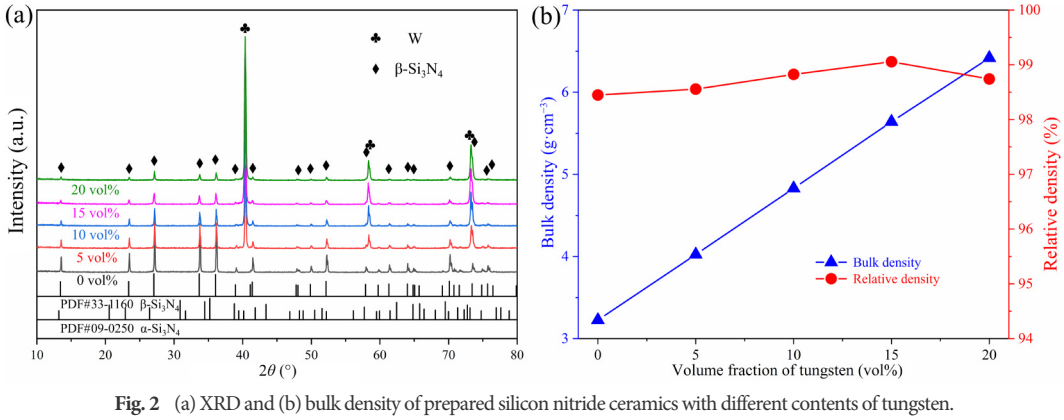

Fig. 2 (a) XRD and (b) bulk density of prepared silicon nitride ceramics with different contents of tungsten.

清华大学出版社 Tsinghua University Press | SciOpen

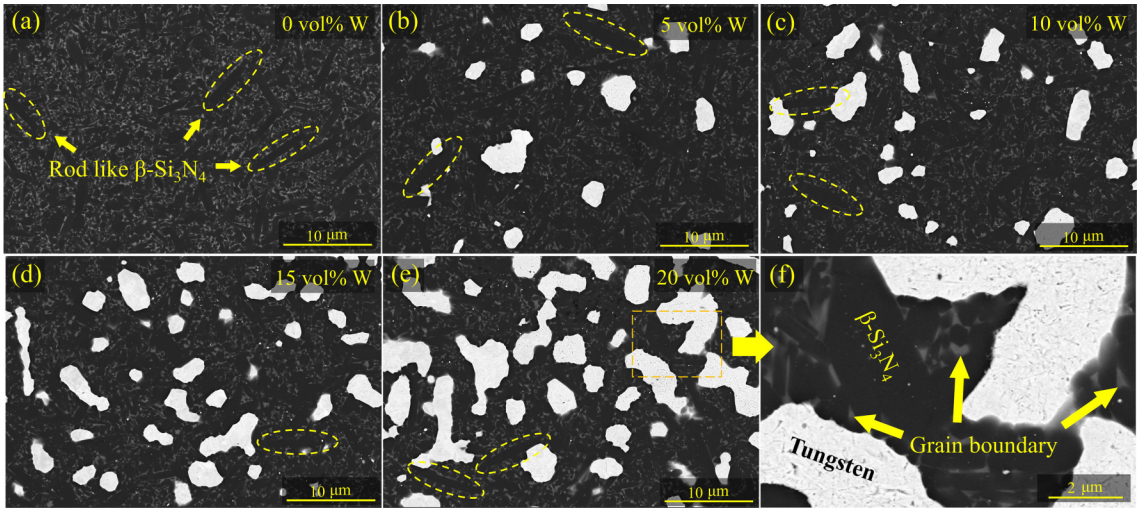

Fig. 3 Backscattered electron SEM images of polished silicon nitride ceramics with different contents of tungsten: (a) monolithic silicon nitride ceramics, (b) 5 vol% tungsten, (c) 10 vol% tungsten, (d) 15 vol% tungsten, (e) 20 vol% tungsten, and (f) partial enlargement in (e).

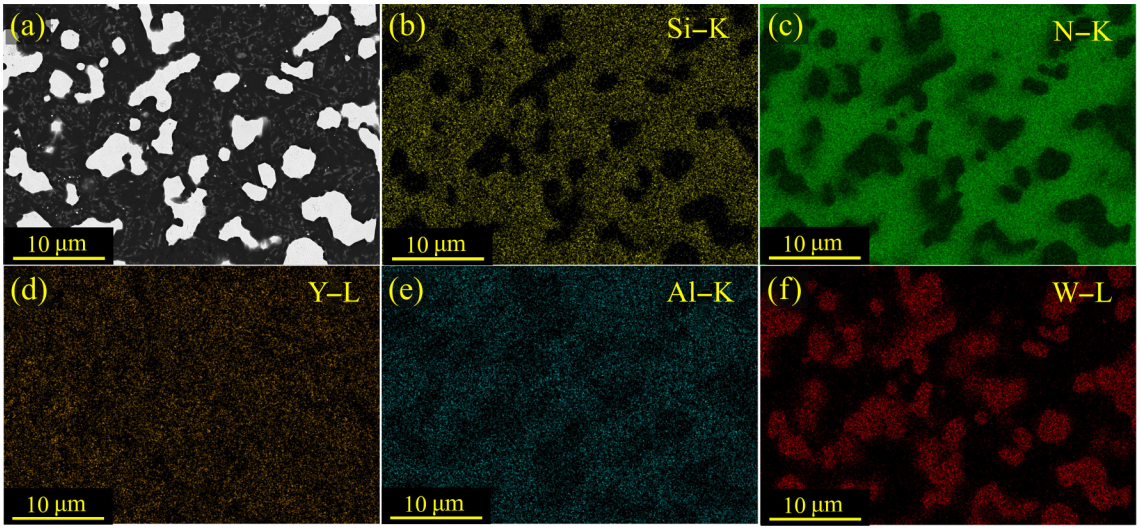

Fig. 4 SEM-EDS mappings of polished silicon nitride ceramics with introduction of 20 vol% tungsten: (a) backscattered electron SEM image and (b–f) EDS of corresponding areas.

observed in the HAADF image, as shown in Fig. 5(a). Energy spectrum analysis near the interface revealed that only tungsten was detected in the tungsten particle area, whereas nitrogen, silicon, and a small amount of oxygen and aluminum were detected in the silicon nitride particle area, as shown in Figs. 5(b) and 5(c). This finding indicates that tungsten did not react with silicon nitride to form tungsten silicide or tungsten nitride. The EDS mappings in Figs. 5(d)–5(f) show that the distributions of tungsten, silicon, and nitrogen are very uniform and that the interface is very clear, which further confirms the above analysis. To further illustrate the forms of the elements present, Figs. 5(g)–5(i) show the selected area electron diffraction patterns of the tungsten particle area, the silicon nitride particle area, and the interface, respectively. By comparison, the diffraction patterns in Figs. 5(g) and 5(h) correspond to the *Im*-3*m* (229) point group of metallic tungsten and the *P*63/*m* (176) point group of β-Si_3N_4, respectively. The diffraction pattern at the interface overlaps, as shown in Fig. 5(i), which further proves that there are no other substances at the interface.

3.2 Thermal expansion and thermal conductivity

The CTE and thermal conductivity of the silicon nitride ceramics are shown in Fig. 6. CTE of monolithic silicon nitride ceramics increases with temperature, and this trend does not change with the introduction of tungsten, as shown in Fig. 6(a). Since the CTE of tungsten is slightly higher than that of silicon nitride ceramics, the CTE of samples increases slightly with increasing tungsten content. Nevertheless, after the introduction of a large amount of tungsten, the composite still maintains a low CTE similar to monolithic silicon nitride ceramics from room temperature (RT) to 1200 °C. The thermal conductivity of silicon nitride ceramics decreases with increasing temperature, as shown in Fig. 6(b). Over the entire temperature range of RT–1000 °C, the introduction of tungsten particles leads to a significant increase in the thermal conductivity of the ceramics. To further analyze the intrinsic mechanism of thermal conductivity enhancement, the specific heat and thermal diffusivity in this temperature range are shown in Figs. 6(c) and 6(d). As the temperature increases, the specific heat and thermal diffusivity of the sample tend to increase and decrease, respectively. After the introduction of tungsten powder, the composition and interface changes cause the specific heat capacity and thermal diffusivity coefficient of the silicon nitride ceramics to fluctuate by approximately 10%–20%, whereas the thermal conductivity almost doubles, as shown in Fig. 6(b).

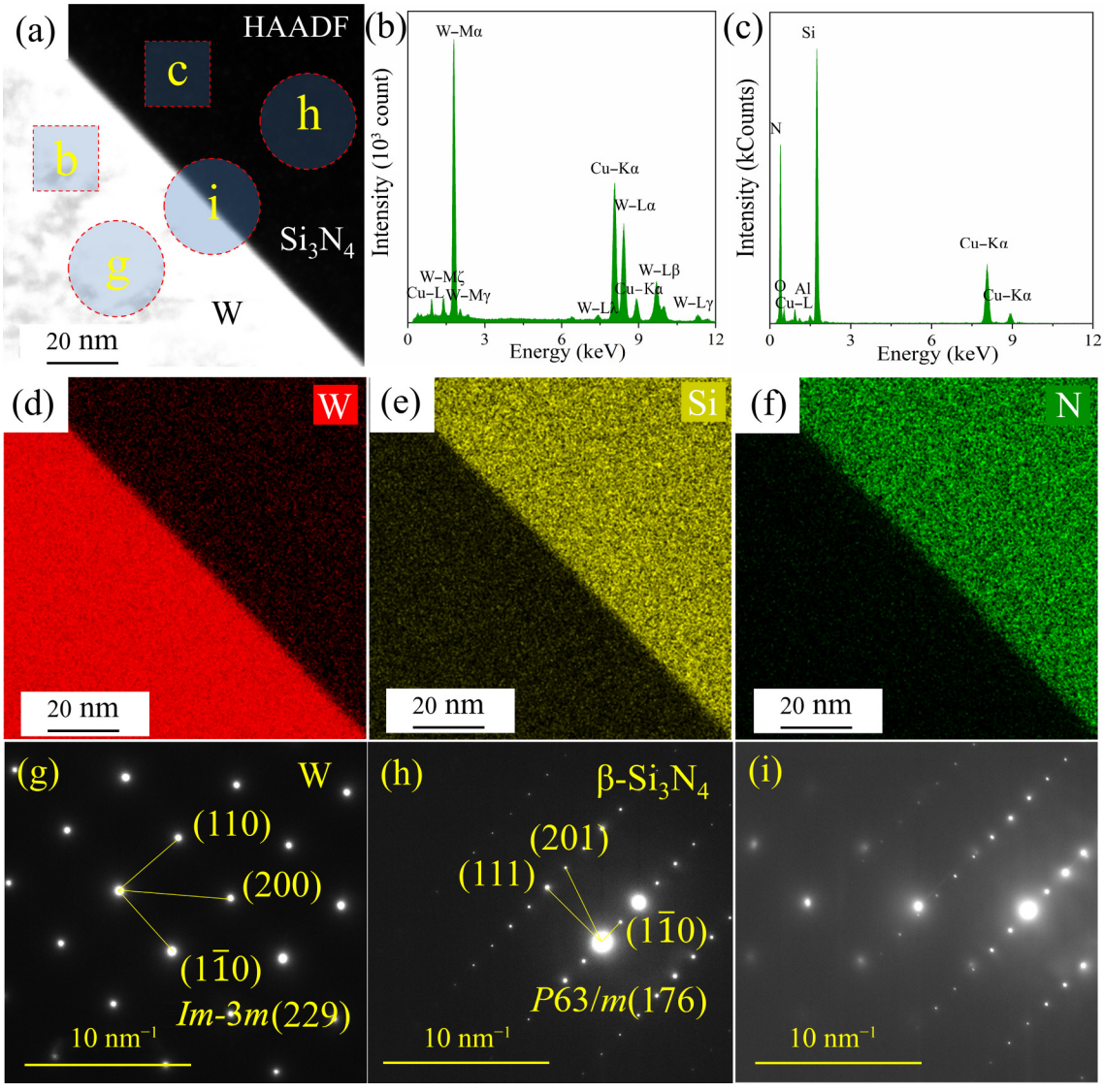

Fig. 5 TEM analysis of polished silicon nitride ceramics with introduction of 20 vol% tungsten: (a) HAADF, (b, c) energy dispersion spectra of corresponding area, (d–f) EDS mappings of whole area, and (g–i) selected area electron diffraction of tungsten particles, silicon nitride particles, and interfaces.

Obviously, the changes in heat capacity and thermal diffusion are not the main reasons for the changes in thermal conductivity. According to the formula, the thermal conductivity of a sample is affected not only by the specific heat and thermal diffusivity but also by its bulk density. With the addition of tungsten, the bulk density of the sample increases gradually, as shown in Fig. 2(b). After introducing 20 vol% tungsten particles, the bulk density of the sample increases from 3.23 to 6.42 g·cm^{-3}, which also results in a nearly doubling of the thermal conductivity of the sample. Therefore, the improvement in the thermal conductivity is due mainly to the increase in the bulk density of the samples caused by the introduction of high-density tungsten particles. Thermal diffusion and specific heat are not significantly affected by the introduction of tungsten.

3.3 Electrical conductivity and permittivity

Figure 7 shows the electrical conductivity and permittivity of the samples. When tungsten particles are not introduced, or the content of tungsten particles does not exceed 15 vol%, the electrical conductivity of the sample is zero, as shown in Fig. 7(a). This finding indicates that tungsten particles have not formed a conductive path and that the composites remain insulating. When the tungsten content reaches 20 vol%, the electrical conductivity of the sample increases significantly. This confirms that the tungsten particle content has reached the percolation threshold, the particles are connected to form conductive paths, and the materials finally achieve conductivity. Although Fig. 3(e) does not show the formation of an obvious fully connected tungsten conductive network, it does show the connections between the tungsten particles. Since it is an SEM image of the polished surface, the three-dimensional conductive network structure cannot be shown in the 2D plane image. This means that the percolation threshold of tungsten in this material system is between 15% and 20% [39]. Achieving conductivity is conducive to the electrical discharge machining (EDM) machinability of this hard material, which is highly beneficial for industrial applications [40]. With the increasing introduction of tungsten particles, the permittivity of the silicon nitride ceramics also changes, as shown in Fig. 7(b). As the tungsten content increases from 5 to 15 vol%, the permittivity of the silicon nitride ceramics increases slightly owing to the increased polarization in the ceramics [41]. When the tungsten content reaches 20 vol%, the permittivity of the ceramics increases significantly in the lower frequency range of 1–30 MHz and exhibits pronounced negative permittivity

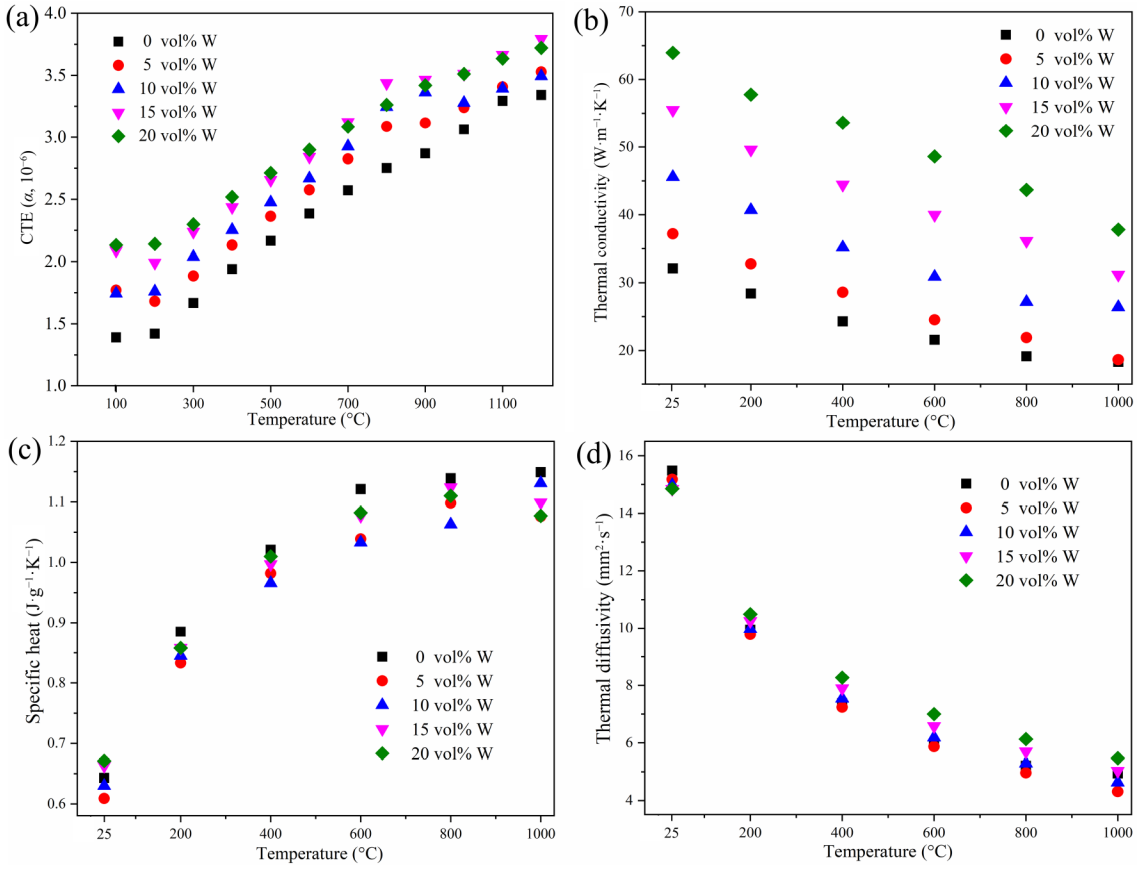

Fig. 6 (a) CTE, (b) thermal conductivity, (c) specific heat, and (d) thermal diffusivity of silicon nitride ceramics with different contents of tungsten.

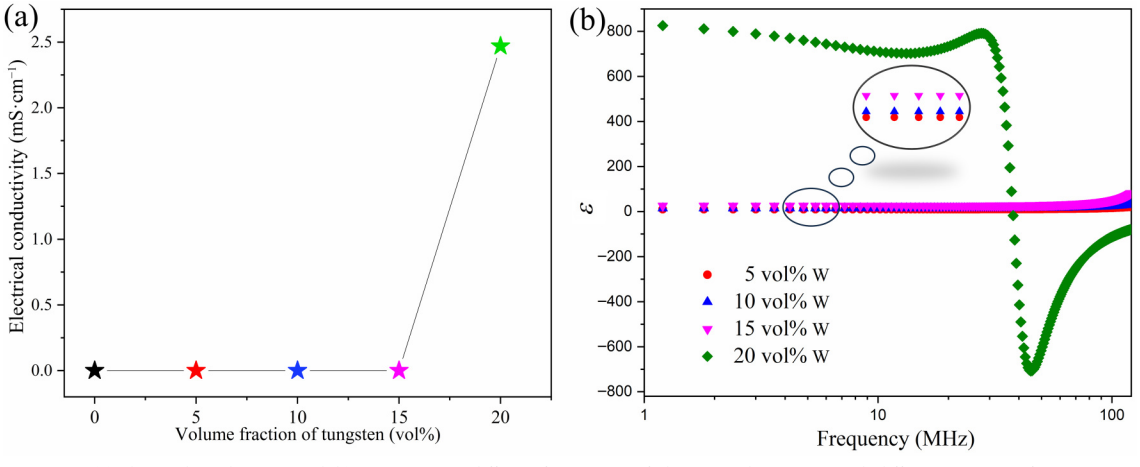

Fig. 7 (a) Electrical conductivity and (b) permittivity at different frequencies of silicon nitride ceramics with different contents of tungsten.

behavior in the frequency range of 40–50 MHz. This plasma-like negative permittivity behavior, which is similar to that of bulk metals, is attributed to the low-frequency plasmonic state stemming from the many unbound electrons in the formed inductive tungsten networks [23].

To further analyze the electrical properties of the silicon nitride ceramics with 20 vol% tungsten, the impedance measurement results are shown in Fig. 8. The impedance-complex impedance spectrum of the sample appears as a semicircle, as shown in Fig. 8(a), indicating that the tungsten particles not only serve as a conductive path in the sample but also form a structure similar to capacitance or inductance in the form of a random distribution. As the frequency increases, the impedance decreases, and the materials exhibit capacitive characteristics, as shown in Fig. 8(b). Complex impedance can generally be considered the difference between inductive reactance and capacitive reactance. At low frequencies, the capacitive reactance is significantly greater than the inductive reactance, and the difference is greatest at approximately 1 MHz, as shown in Fig. 8(c). As the frequency increases, the difference gradually decreases, which is due to the decrease in the capacitive reactance and the increase in the inductive reactance with increasing AC frequency. When the frequency is in the range of 40–50 MHz, the capacitive and inductive reactance are essentially equal, resulting in resonance, that is, plasma resonance, which is the cause of the negative permittivity behavior observed in Fig. 7(b). Dielectric resonance was the cause of the negative permittivity behavior. As the AC frequency continues to increase, the inductive reactance becomes

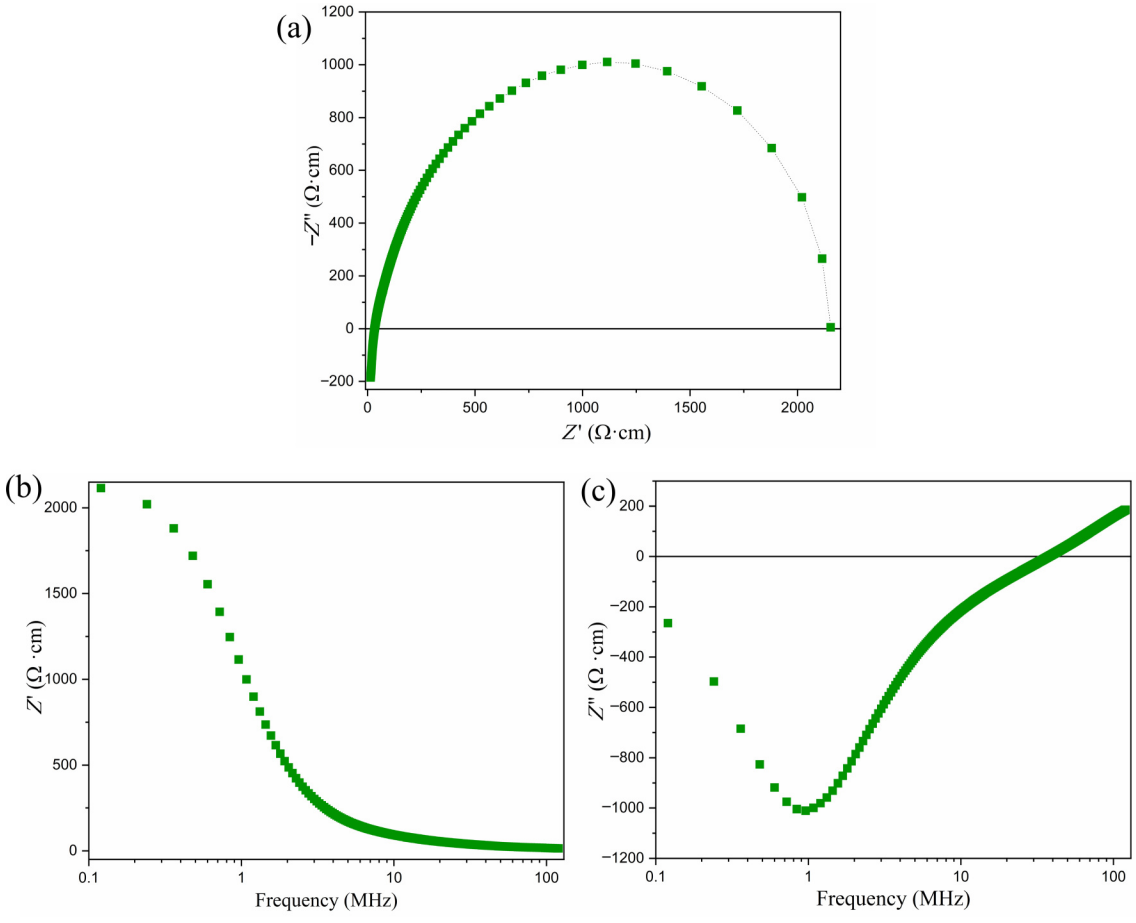

Fig. 8 Impedance complex plane plots of silicon nitride ceramics with 20 vol% tungsten.

greater than the capacitive reactance, the resonance weakens, and the negative permittivity behavior gradually disappears.

This negative permittivity behavior has great potential for applications in the fields of electromagnetic shielding, subwavelength imaging, optical cloaking, wave filtering, superlenses, and band gap design [17]. Similar phenomena have also been observed by introducing other conductive particles into silicon nitride ceramics [22–27]. Nevertheless, the current preparation methods for silicon nitride-based metamaterials are limited to pressure-assisted sintering [26] or impregnation of porous ceramics [22–24,27]. Compared with samples prepared by impregnation processes, which often have high porosity for the solution to penetrate [22–24], pores are almost absent in these materials. The high density gives these materials great advantages in terms of strength, hardness, wear resistance, oxidation resistance, corrosion resistance, etc., and they can adapt to harsh service environments. Under a mechanical-assisted sintering process such as SPS, densification can be achieved at a lower temperature or shorter time to reduce the melting agglomeration of the second metal phase [42], and densification of silicon nitride ceramics can also be achieved when the sintering activity becomes worse after the introduction of carbon materials [1]. However, in this case, the grain growth and even phase transformation of silicon nitride cannot be completed [25,26], and the production efficiency is severely limited. It is generally believed that a certain number of large-sized β-Si_3N_4 grains are the key to the higher fracture toughness of silicon nitride ceramics than other ceramics [43]. As discussed above, in this materials, all α-Si_3N_4 was transformed to β-Si_3N_4, and β-Si_3N_4 grains grew to a certain extent under this process, as shown in Fig. 3, which is very beneficial for maintaining the high fracture toughness advantage of silicon nitride ceramics. In addition, good thermal conductivity and a low thermal expansion coefficient also allow the materials to remain stable after Joule heat is generated inside during service. More importantly, metamaterials are densified by gas pressure sintering, which can meet the requirements of complex shapes and high efficiency in industrialization. Overall, this work proposes a dense silicon nitride-based metamaterials with industrial potential.

4 Conclusions

To overcome the performance and industrialization limitations of current silicon nitride-based metamaterials, new silicon nitride-based metamaterials were proposed and prepared. Silicon nitride ceramics with different tungsten contents ranging from 0 to 20 vol% were prepared via gas pressure sintering. All the samples were fully densified regardless of the tungsten content by applying a flowing nitrogen atmosphere during the sintering process. Since the CTEs of tungsten and silicon nitride are similar, the composites maintain a low CTE even after a high content of tungsten is introduced. Tungsten particles significantly improve the thermal conductivity of composites, which is mainly due to the increase in bulk density. When tungsten particles are not introduced or the content of tungsten particles does not exceed 15 vol%, the silicon nitride ceramics remain insulating and have a low permittivity. After 20 vol% tungsten was introduced, the tungsten particles interconnected to form conductive pathways, and the composite became conductive. In addition, the random distribution of tungsten particles significantly changed the permittivity of the composites, and a negative permittivity

behavior was observed in the frequency range of 40–50 MHz. A dense silicon nitride-based metamaterials with industrial potential was proposed and prepared, guiding the industrial exploration and application of high-performance metamaterials.

Acknowledgements

This work was supported by the National Natural Science Foundation of China (No. 52102080), the Youth Science Foundations of Gansu Province (No. 23JRRA598), and the Shandong Provincial Natural Science Foundation (Nos. ZR2020ZD29 and ZR2021JQ20).

Declaration of competing interest

The authors have no competing interests to declare that are relevant to the content of this article. The author Dewei Ni is the Editorial Committee member of this journal.

References

[1] Li YX, Han WB, Chen GQ, *et al.* The Microstructure and thermal diffusivity of carbon nanostructures/Si_3N_4 composites processed using spark plasma sintering. *Ceram Int* 2017, **43**: 3435–3438.
[2] Riley FL. Silicon nitride and related materials. *J Am Ceram Soc* 2000, **83**: 245–265.
[3] Tang SJ, Guo WM, Sun SK, *et al.* Design strategy of phase and microstructure of Si_3N_4 ceramics with simultaneously high hardness and toughness. *J Adv Ceram* 2023, **12**: 122–131.
[4] Li W, Yu ZJ, Wiehl L, *et al.* Hard and tough novel high-pressure γ-Si_3N_4/Hf_3N_4 ceramic nanocomposites. *J Adv Ceram* 2023, **12**: 1418–1429.
[5] Liu S, Liu W, Man Y, *et al.* Study on thermal shock resistance and attenuation law of silicon nitride ceramic materials at high temperature. *Adv Ceram* 2023, **44**: 451–460.
[6] Zhang W, Su L, Lu D, *et al.* Resilient Si_3N_4@SiO_2 nanowire aerogels for high-temperature electromagnetic wave transparency and thermal insulation. *J Adv Ceram* 2023, **12**: 2112–2122.
[7] Fukuda Y, Harada K, Yonetsu M, *et al.* Relation between crystal structure and lattice oxygen content of sintered reaction-bonded silicon nitride. *J Am Ceram Soc* 2021, **104**: 6563–6571.
[8] Li JS, Yu QP, Li D, *et al.* Formation of hierarchical Si_3N_4 foams by protein-based gelcasting and chemical vapor infiltration. *J Adv Ceram* 2021, **10**: 187–193.
[9] Nag A, Rao RR, Panda PK. High temperature ceramic radomes (HTCR)—A review. *Ceram Int* 2021, **47**: 20793–20806.
[10] Wu JM, Zhang XY, Xu J, *et al.* Preparation of porous Si_3N_4 ceramics via tailoring solid loading of Si_3N_4 slurry and Si_3N_4 poly-hollow microsphere content. *J Adv Ceram* 2015, **4**: 260–266.
[11] Xu SS, Zhou XN, Zhi Q, *et al.* Anisotropic, biomorphic cellular Si_3N_4 ceramics with directional well-aligned nanowhisker arrays based on wood-mimetic architectures. *J Adv Ceram* 2022, **11**: 656–664.
[12] Chen SL, Wang L, He G, *et al.* Microstructure and properties of porous Si_3N_4 ceramics by gelcasting-self-propagating high-temperature synthesis (SHS). *J Adv Ceram* 2022, **11**: 172–183.
[13] Kadic M, Milton GW, van Hecke M, *et al.* 3D metamaterials. *Nat Rev Phys* 2019, **1**: 198–210.
[14] Luo Y, Estevez D, Scarpa F, *et al.* Microwave properties of metacomposites containing carbon fibres and ferromagnetic microwires. *Research* 2019, **2019**: 3239879.
[15] Gholipur R, Khorshidi Z, Bahari A. Enhanced absorption performance of carbon nanostructure based metamaterials and tuning impedance matching behavior by an external AC electric field. *ACS Appl Mater Inter* 2017, **9**: 12528–12539.
[16] Li B, Sui G, Zhong W. Single negative metamaterials in unstructured polymer nanocomposites toward selectable and controllable negative permittivity. *Adv Mater* 2009, **21**: 4176–4180.
[17] Muhammad, Lim CW. From photonic crystals to seismic metamaterials: A review via phononic crystals and acoustic metamaterials. *Arch Comput Method E* 2022, **29**: 1137–1198.
[18] Luo WJ, Wang S, Zheng SY, *et al.* Dielectric response of ANb_2O_6 (A = Zn, Co, Mn, Ni) columbite niobates: From microwave to terahertz. *J Adv Ceram* 2024, **13**: 1189–1197.
[19] Wu P, Zeng YP, Wang J, *et al.* Realizing microwave-infrared compatible stealth via single 8YSZ coating. *J Adv Ceram* 2024, **13**: 1535–1545.
[20] Wood J. The top ten advances in materials science. *Mater Today* 2008, **11**: 40–45.
[21] Xie PT, Shi ZC, Feng M, *et al.* Recent advances in radio-frequency negative dielectric metamaterials by designing heterogeneous composites. *Adv Compos Hybrid Mater* 2022, **5**: 679–695.
[22] Cheng CB, Yan KL, Fan RH, *et al.* Negative permittivity behavior in the carbon/silicon nitride composites prepared by impregnation-carbonization approach. *Carbon* 2016, **96**: 678–684.
[23] Cheng CB, Jiang YL, Sun X, *et al.* Tunable negative permittivity behavior and electromagnetic shielding performance of silver/silicon nitride metacomposites. *Compos Part A Appl S* 2020, **130**: 105753.
[24] Cheng CB, Fan RH, Wang ZY, *et al.* Tunable and weakly negative permittivity in carbon/silicon nitride composites with different carbonizing temperatures. *Carbon* 2017, **125**: 103–112.
[25] Cheng CB, Fan RH, Wang ZY, *et al.* Radio-frequency negative permittivity in the graphene/silicon nitride composites prepared by spark plasma sintering. *J Am Ceram Soc* 2018, **101**: 1598–1606.
[26] Cheng CB, Liu YH, Shi SJ, *et al.* Negative permittivity behavior in carbon fibre/silicon nitride ceramic composites prepared by spark plasma sintering. *Ceram Int* 2021, **47**: 35201–35208.
[27] Zhang ZD, Cheng CB, Han X. Percolative cobalt/silicon nitride composites with tunable negative electromagnetic parameters. *RSC Adv* 2016, **6**: 82478–82483.
[28] Xu CQ, Qu YP, Fan GH, *et al.* Tunable and weakly negative permittivity at radio frequency range based on titanium nitride/polyethylene terephthalate composites. *J Mater Sci Mater El* 2018, **29**: 15994–16003.
[29] Wang LJ, Qi Q, Zheng JQ, *et al.* A novel thermally matched conductive phase of silicon nitride ceramics. *J Phys Chem Solids* 2023, **179**: 111379.
[30] Wei ZL, Liu SY, Liu DG, *et al.* Fabrication and properties of symmetrical W/Si_3N_4/W functionally graded materials by spark plasma sintering. *J Alloys Compd* 2022, **896**: 163077.
[31] Wang LJ, Qi Q, Zhang H, *et al.* The fabrication of tungsten reinforced silicon nitride ceramics by altering nitrogen pressure. *Ceram Int* 2019, **45**: 5927–5931.
[32] Wang LJ, Qi Q, Zhang H, *et al.* High tough W-added silicon nitride ceramics. *Ceram Int* 2019, **45**: 19055–19059.
[33] Wang LJ, Qi Q, Wang ZY, *et al.* The effect of tungsten introduction on the tribological properties of Si_3N_4 ceramics paired with GCr15 steel under nonlubricated conditions. *Wear* 2022, **506**: 204452.
[34] Wang LJ, Qiao ZH, Qi Q, *et al.* Improving abrasive wear resistance of Si_3N_4 ceramics with self-matching through tungsten induced tribochemical wear. *Wear* 2022, **494**: 204254.
[35] Hyuga H, Jones MI, Hirao K, *et al.* Mechanical and wear properties of Si_3N_4–W composites using tungsten boride powder. *J Mater Res* 2003, **18**: 2262–2267.
[36] Flower GL, Baskaran GS, Mohan NK, *et al.* The structural role of tungsten ions in PbO–Sb_2O_3–As_2O_3 glass-system by means of spectroscopic investigations. *Mater Chem Phys* 2006, **100**: 211–216.
[37] Rao CS, Ravikumar V, Srikumar T, *et al.* The role of coordination and valance states of tungsten ions on some physical properties of Li_2O–Al_2O_3–ZrO_2–SiO_2 glass system. *J Non-Cryst Solids* 2011, **357**: 3094–3102.
[38] Wegener T, Klein F, Litnovsky A, *et al.* Development of yttrium-containing self-passivating tungsten alloys for future fusion power plants, *Nucl Mater Energy* 2016, **9**: 394–398.

[39] Kováčik J. Electrical conductivity of two-phase composite material. *Scripta Mater* 1998, **39**: 153–157.
[40] Zhao J, Zhang XS, Ma ZN, *et al*. Tuning mechanical and electrical performances of B_4C–TiB_2 ceramics in a two-step spark plasma sintering process. *J Adv Ceram* 2024, **13**: 518–528.
[41] Qing YC, Wen QL, Luo F, *et al*. Temperature dependence of the electromagnetic properties of graphene nanosheet reinforced alumina ceramics in the X-band. *J Mater Chem C* 2016, **4**: 4853–4862.
[42] Liu JJ, Wang ZX, Yin B, *et al*. A novel method to prepare self-lubricity of Si_3N_4/Ag composite: Microstructure, mechanical and tribological properties. *J Am Ceram Soc* 2018, **101**: 3745–3748.
[43] Becher PF, Sun EY, Plucknett KP, *et al*. Microstructural design of silicon nitride with improved fracture toughness: I, effects of grain shape and size. *J Am Ceram Soc* 1998, **81**: 2821–2830.